Single Molecular Catalysis Identifying Activation Energy of Intermediate Product and Rate-limiting Step in Plasmonic Photocatalysis

Wei Li[1,2], Junjian Miao[4], Tianhuan Peng[1,5], Hui Lv[1,2], Jun-Gang Wang[3], Kun Li[5], Di Li*[,3]

[1] Division of Physical Biology and Bioimaging Center, Shanghai Synchrotron Radiation Facility, Shanghai Institute of Applied Physics, Chinese Academy of Sciences, Shanghai 201800, China

[2] University of Chinese Academy of Sciences, Beijing 100049, China

[3] School of Chemistry and Molecular Engineering, East China Normal University, Shanghai 200241, China

[4] College of Food Science and Technology, Shanghai Ocean University, Shanghai 201306, P. R. China

[5] State Key Laboratory of Chemo/Biosensing and Chemometrics, College of Chemistry and Chemical Engineering, Hunan Provincial Key Laboratory of Biomacromolecular Chemical Biology, Hunan University, Changsha 410082, P. R. China

ABSTRACT

Plasmon mediated photocatalysis provides a novel strategy for harvesting solar energy. Identification of rate determining step and its activation energy in plasmon mediated photocatalysis plays critical roles for understanding the contribution of hot carriers that facilitates rational designing catalysts with integrated high photo-chemical conversion efficiency and catalytic performance. However, it remains a challenge due to a lack of research tools with spatiotemporal resolution that capable of capturing intermediates. In this work, we used a single molecular fluorescence approach to investigate a localized surface plasmon resonance (LSPR) enhanced photocatalytic reaction with sub-turnover resolution. By introducing variable temperature as an independent parameter in plasmonic photocatalysis, the activation energies of tandem reaction steps, including intermediate generation, product generation and product dissociation, were clearly differentiated, and intermediates generation was found to be the rate-limiting step. Remarkably, the cause of plasmon enhanced catalysis performance was found to be its ability of lowering the activation energy of intermediates generation. This study gives new insight into the photo-chemical energy conversion pathways in plasmon enhanced photocatalysis and sheds light on designing high performance plasmonic catalysts.

Plasmonic photocatalysis by making use of localized surface plasmonic resonance (LSPR) of noble metal nanoparticles (NPs) has emerged as a promising approach to facilitate light-driven chemical conversions.[1-4] Hot charge carriers, including hot electrons and hot holes, generated by plasmonic illuminations play synergistic roles in enhancing catalytic performance.[5-7] However, determining activation energies and rate limiting step under illumination condition and exploring the contribution of hot carrier reduced activation barrier is still rare and controversy.[1,8] For example, El-Sayed and coworkers found that the activation barrier for hexacyanoferrate (III) reduction on Au NPs was slightly higher under visible light excitation than that in the dark, even though the reaction rate was accelerated under light.[9] While for the same reaction, Jain et al. suggested the activation enthalpy was reduced under light excitation.[10] Zhu and coworkers demonstrated an appreciable reduction in activation energy when light excitation was employed for cross-coupling reactions on Au/Pd alloy NPs.[11-12] These controversy indicates elaborated characterizations are needed to obtain precise activation energy of tandem catalytic steps and to determine rate-limiting step in plasmonic photocatalysis, which will provide new understandings of the role of hot carriers in plasmon-mediated photochemistry.

Single-molecule fluorescence microscopy (SMFM) has been proved as a powerful tool in operando investigating elementary chemical reactions on single catalyst.[13-17] One unique advantage of single molecular approach in exploring nanocatalysis is its capability to divide a catalytic turnover into product formation process and dissociation process.[18-19] With this sub-turnover resolution, it possesses great potential for obtaining the thermodynamic and kinetic information of each reaction sequences that unavailable from ensemble measurements. Recently, Xu et al. introduced temperature as an independent variable into single-molecule nanocatalysis, and for the first time obtained the corresponding activation energies for both product formation and dissociation processes of a fluorogenic reaction.[20]

Compared with thermal catalysis that involves only chemical transformation,

plasmonic photocatalysis also involves an excitation of hot charge carriers and the transmission of hot carriers from plasmonic nanostructures to the adsorbed reactants.[21] Thereby, plasmonic photocatalysis contains two or more elementary reactions, and at least one intermediate was involved.[22] As a result, It is more complicated to identify the rate-limiting step in plasmonic photocatalysis. In the present study, we employed SMFM to investigate an Au nanorods (NRs) catalyzed reaction under plasmonic activation. By changing temperature, the temperate-dependent plasmonic photocatalytic reaction was studied with sub-turnover resolution. Through statistical analysis of single turnovers, activation energy of rate-limiting step of the plasmonic photocatalytic reaction was identified. Remarkably, we found that the plasmon excitation lowers the activation energy for intermediates generating. This study exemplifies a new function of single molecule catalysis in exploring the mechanism of hot carriers enhanced photocatalytic reactions for designing high performance photocatalysts.

Results and Discussion

Plasmon-Enhanced Au Nanorods Catalyzed Fluorogenic Reaction

A classical plasmonic metal NPs catalyzed fluorogenic oxidation reaction between nonfluorescent Amplex Red (AR) and H_2O_2 was chosen as a model to exemplify the plasmon enhancement. An independent parameter, reaction temperature, was introduced to obtain the activation energies of tandem reaction steps. The scheme of experimental setup is shown in Figure 1A. A home-build temperature controllable microfluidic flow cell equipped with recycling water bath was used as reactor. Au NRs with aspect ratio of 3.6 and longitudinal LSPR peak at 785 nm was used as catalysts (Figure 1B). A 785 nm laser was introduced to illuminate the reactor to excite Au nanorods. In order to avoid overlap of LSPR wavelength of Au NPs with excitation wavelength of fluorescent product Resorufin (Rf, excitation wavelength at 561 nm), Au NRs were adopted as plasmon photocatalysts rather than Au NPs.

We first investigated the Au NRs catalyzed fluorogenic reaction at room temperature under dark or laser illumination. The fluorescent product Rf generated on

a single Au NR was real-time monitored by total internal reflection fluorescence microscope (TIRFM) with a temporal resolution of 30 ms/frame (Figure 1D). The digital fluorescence on-off burst in Figure 1D is a characteristic of single molecule catalysis. Of note, the fluorescence intensity of on level was not identical, which was attributed to the presence of multiple catalytic sites on one Au NR. Moreover, several control experiments were performed to confirm the occurring of the single molecule catalysis on single nanocatalyst. These include: (1) no stochastic fluorescence bursts were observed in the absence of either Au NRs or reaction substrates (AR and H_2O_2), indicating the fluorescence burst is a result of catalytic reaction (Figure S1); (2) no digital fluorescence bursts were observed when Rf solution was flowed over Au NRs under the same experiment condition, suggesting the fluorescence burst is not resulting from binding/unbinding of free Rf to Au NRs (Figure S2); (3) the fluorescence burst frequencies were independent of 561 nm laser intensity (Figure S3); (4) the average time scale of fluorescence on is less than 0.2 s, which is much shorter than the average photobleaching lifetime of Rf molecule (ca. 25 s) under similar laser intensity.[13] Therefore, we convince ourselves that each sudden fluorescence burst represents the generation of a Rf molecule on single Au NR.

In these single-molecule fluorescence trajectories, photocatalytic events contain two stochastic waiting times, τ_{off} and τ_{on}, representing the time before each Rf formation and then dissociation from Au NRs, respectively. The inverse of τ_{off} and τ_{on} thus represent the reaction rate for product generation and dissociation. Interestingly, under 785 nm laser illumination, the appearance frequency of fluorescence burst was increased (Figure 1D and Figure S4). We calculated the average $<\tau_{off}>^{-1}$ and $<\tau_{on}>^{-1}$ (< > denotes average) from 50 trajectories under dark or laser illumination, respectively. Under 785 nm laser illumination, the average product generation rate ($<\tau_{off,\ light}>^{-1}$) was calculated to be 2.1 ± 0.4 s^{-1}, which was 3 times faster than that under the dark ($<\tau_{off,\ dark}>^{-1}$, 0.7 ± 0.3 s^{-1}) (Figure 1E). While for the product dissociation rate, $<\tau_{on,\ light}>^{-1}$ (10.3 ± 0.9 s^{-1}) was also about 1.3 times faster than $<\tau_{on,\ dark}>^{-1}$ (8.1 ± 0.8 s^{-1}) (Figure 1E). The comparison of single molecule product generation and dissociation rate

clearly supported the plasmonic enhancement. In addition, we also compared the catalytic reaction of bulk solution under dark or laser illumination, and found similar plasmonic enhanced performance (Figure S5), further confirming the solidity of single molecular measurements.

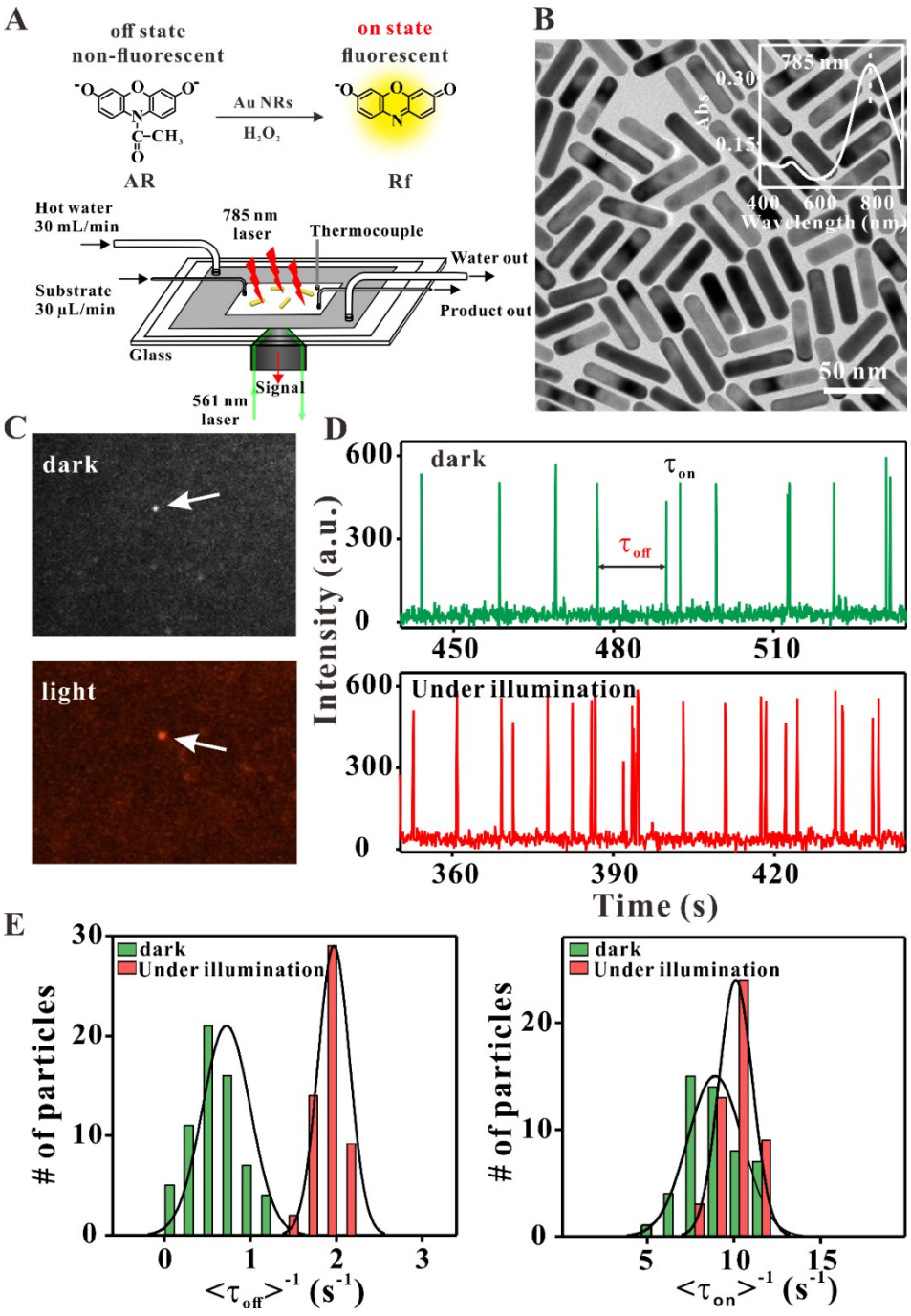

Figure 1. Plasmon enhanced photocatalysis on single Au NR. (A) Schematic illustrating the individual Au NRs catalyzed fluorogenic reaction under 785 nm laser illumination with temperature control setup. (B) TEM image of Au NRs, inset: UV-vis spectrum of Au NRs. (C)

Typical TIRFM images of single Rf molecule generated on single Au NRs under dark (top) or laser illumination (bottom) at 298 K in the presence of 400 nM AR and 88.3 mM H_2O_2. (D) Typical fluorescence trajectories recorded from the fluorescent spots marked with arrows in (C). (E) Comparison of $<\tau_{off}>^{-1}$ (left) and $<\tau_{on}>^{-1}$ (right) derived from fluorescence trajectories under dark or laser illumination. Solid lines are fit with Gaussian function.

Single Molecular Measurements Identify Intermediate and Rate-Limiting Step under Dark

Having confirmed the Au NRs catalyzed fluorogenic reaction could be enhanced by plasmon, we then attempted to capture intermediate products by harnessing the single molecular kinetical analysis. As shown in Figure 1E, the product generation rate ($<\tau_{off}>^{-1}$) is much smaller than its dissociation rate ($<\tau_{on}>^{-1}$) under either dark or laser illumination, indicating that rate-limiting of this reaction is involved in the product generation step.

The reaction mechanism between AR and H_2O_2 has been extensively studied.[23-24] Substrate AR is first oxidized to a nonfluorescent intermediate product AR and then converted into final fluorescent product Rf with reaction rate constants of k_1 and k_2, respectively (Figure 2A). However, kinetics of individual step is unavailable from ensemble measurements and thereby hard to identify the rate-limiting step. τ_{off} in fluorescence trajectory thus involves the reaction time required for the oxidation of AR to AR$\cdot$, and then to Rf. Of note, H_2O_2 was kept large excess, thus the reaction can be considered as a quasi-first order reaction of AR. Figure 2B shows the distribution of τ_{off} from a single Au NR (more details in supplementary information and Figure S6). Obviously, the distribution of τ_{off} follows a quick rise and then gradual decay. This rise and decay distribution of τ_{off} indicated that the formation the fluorescent product contains at least two sequential steps and a hidden kinetic intermediate,[24-25] which coincides with previous mechanism explorations.[26] To further verify the kinetic intermediate, we investigated a control N-deoxygenation reaction of Resazurin to Resorufin (Figure 2C). This reaction mechanism is identified as a single step reduction.[27] In sharp contrast to the τ_{off} distribution shown in Figure 2B, τ_{off} of the deoxygenation reaction follows a single exponential decay distribution (Figure 2D).

Therefore, we concluded the rise-decay behavior of τ_{off} in Figure 2B indeed contains at least two sequential reaction steps.

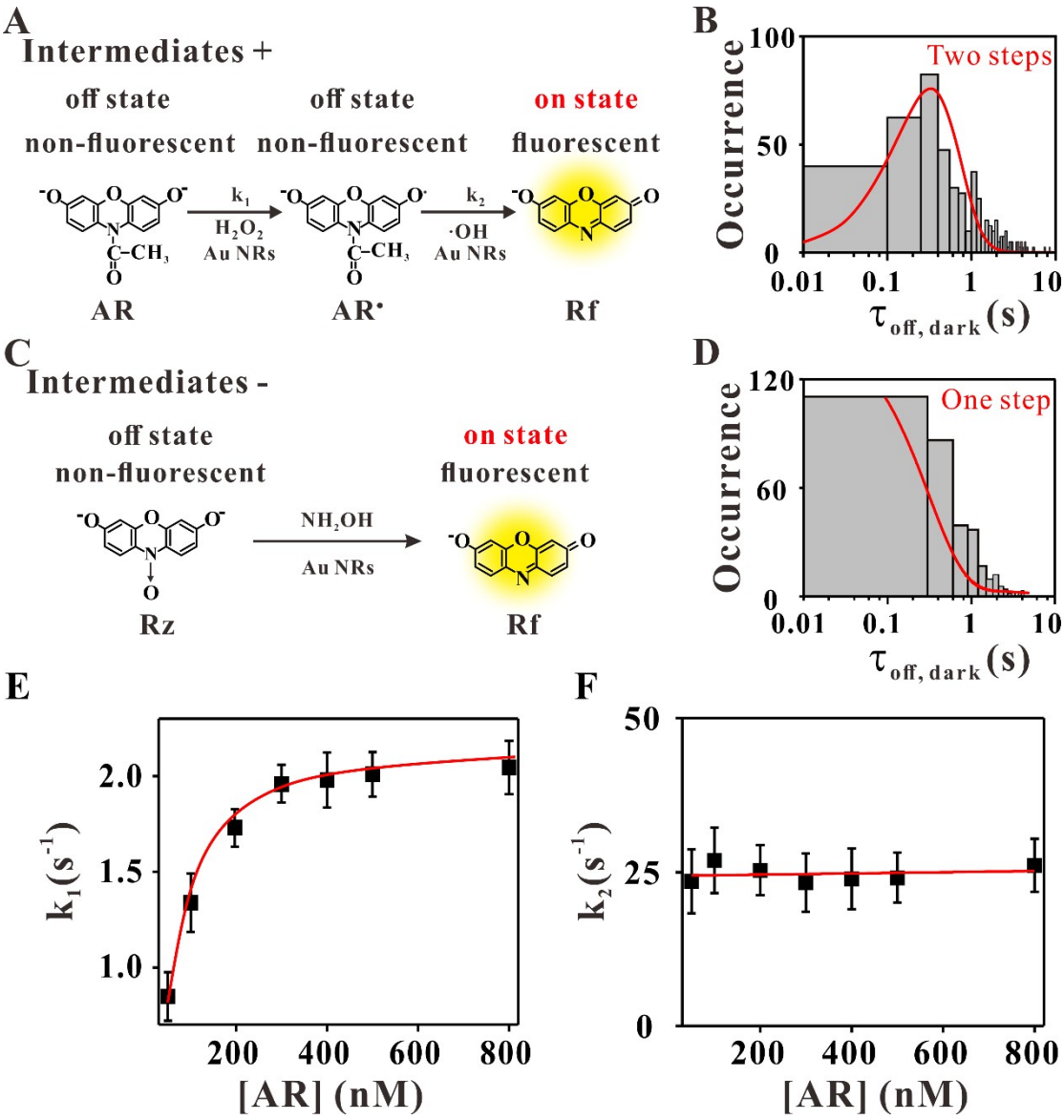

Figure 2. Identification the rate-limiting step of the fluorogenic reaction under dark. (A) Reaction mechanism of oxidative deacetylation of Amplex Red to Resorufin. (B) Distribution of $\tau_{off,\ dark}$ for the oxidative deacetylation reaction from a single Au NR in the presence of 400 nM AR and 88.3 mM H_2O_2. Red lines are empirical fit with $y = A\left(1 - k_1\tau - e^{-k_2\tau}\right)$ (a simplified form of Eq. 1). (C) Reaction mechanism of reductive N-deoxygenation of Resazurin to Resorufin. (D) Distribution of $\tau_{off,\ dark}$ for the reductive N-deoxygenation reaction from a single Au NR in the presence of 50 nM Rz and 180 μM NH_2OH. Red lines are empirical fit with $y = Ae^{-k\tau}$. (E) and (F) Dependence of the apparent rate constant k_1(E) and k_2 (F) on [AR] from the same Au NRs.

We next investigated the single molecule kinetics of each step to identify rate-

limiting step. Based on noncompetitive Langmuir−Hinshelwood mechanism, the probability density function *f(τ)* of τ_{off} can be derived as:

$$f(\tau)=\frac{k_1 k_2}{k_2-k_1}\left(e^{-k_1\tau}-e^{-k_2\tau}\right) \qquad (1)$$

where k_1 and k_2 are the corresponding apparent rate constants of intermediate product formation and final product formation (Figure 2A), respectively.[24] k_1 and k_2 can take the following forms when H_2O_2 concentration was kept large excess:

$$k_1[H]\underset{\rightarrow}{\rightarrow}\infty\gamma_{eff1}G_A[A]/\left(1+G_A[A]\right) \qquad (2)$$

$$k_2[H]\underset{\rightarrow}{\rightarrow}\infty\gamma_{eff2} \qquad (3)$$

where G_A is the adsorption equilibrium constant of AR, γ_{eff1} and γ_{eff2} are the effective rate constants of intermediate product formation and final product formation, respectively, [A] represents the concentration of the substrate AR, [H] represents the concentration of H_2O_2.[24]

We then analyzed multiple fluorescence trajectories to derive k_1 and k_2 (Figure 2E and F), each point in Figure 2E and F was averaged over multiple fluorescence trajectories and the solid lines were fits with Eq. 2 or 3. We found that k_1 was dependent on [AR] and reached plateau when [AR] was higher than 400 nM (Figure 2E), while k_2 was independent of [AR] and remained unchanged (Figure 2F). The calculated k_2 was one order of magnitude higher than k_1, indicating that AR· formation is the rate-limiting step in the product generation.

Identification of the Activation Energy of Rate-limiting Step in Plasmonic Photocatalysis

The apparent activation energy of each reaction step ($E_{a,i}$) could be obtained from the Arrhenius equation;

$$k_i=A_i e^{-E_{a,i}/\mathrm{RT}} \qquad (4)$$

where k_i is the rate constant and A_i is the preexponential factors of step *i*.

Taking into consideration that k_1 and k_2 could be simplified as $k_1 \rightarrow \gamma_{eff1}$, $k_2 \rightarrow \gamma_{eff2}$

when [AR] = 400 nM and H_2O_2 was large excess, Eq. 4 could be deduced to:

$$\ln\left(k_1\right)=\ln\left(\gamma_{\text{eff1}}\right)=\ln\left(A_{\text{off1}}\right)-E_{a,\text{off1}}/\text{RT} \quad (5)$$

$$\ln\left(k_2\right)=\ln\left(\gamma_{\text{eff2}}\right)=\ln\left(A_{\text{off2}}\right)-E_{a,\text{off2}}/\text{RT} \quad (6)$$

$$\ln\left(\left\langle\tau_{\text{on}}\right\rangle^{-1}\right)=\ln\left(k_3\right)=\ln\left(A_{on}\right)-E_{a,\text{on}}/\text{RT} \quad (7)$$

where A_{off} and A_{on} represent the preexponential factor of the surface process occurred in τ_{off} and τ_{off}, respectively, $E_{\text{a,off1}}$, $E_{\text{a,off2}}$ and $E_{\text{a,on}}$ are the activation energy for intermediate product formation process, final product formation and final product dissociation process, respectively, k_3 is the rate constant of final product dissociation.

We then monitored the temperature-dependent catalytic reaction under dark or 785 nm laser illumination to derive the activation energies of different tandem reaction steps. By extracting τ_{off} in each trajectory, the rate constants γ_{eff1} and γ_{eff2} at different temperature could be derived by fitting the distributions of τ_{off} with eq. 1 (Table S1). Therefore, the activation energy for intermediate formation ($\langle E_{a,\ \text{off1}}\rangle$), final product formation ($\langle E_{a,\ \text{off2}}\rangle$) and product dissociation process ($\langle E_{a,\ \text{on}}\rangle$) were derived from Eq. 5-7 and demonstrated in Figure 3C and Table 1.

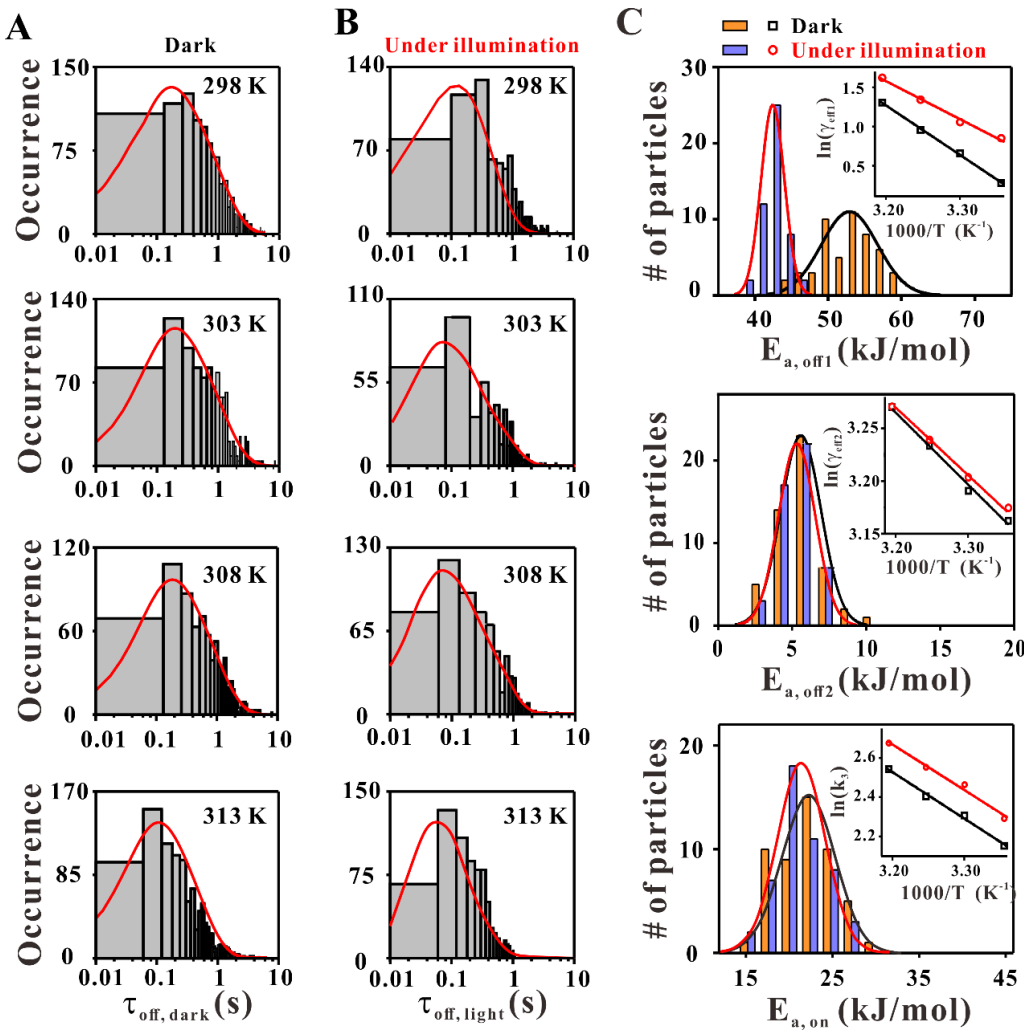

Figure 3. Identification the activation energies of tandem reaction steps during in plasmon photocatalytic reaction. Distributions of τ_{off} under dark (A) or laser illumination (B) from single Au NR at different temperatures in the presence of 400 nM AR and 83.3 mM H_2O_2. Solid red lines are empirical fits of Eq 1. (C) The distribution of $E_{a\ i}$ for intermediate formation process (top), final product formation process (medium) and product dissociation process (bottom) calculated from over 100 Au NRs. Insets: the average Arrhenius plots under dark (black rectangle, □) or laser illumination (red circle, ○) over 100 Au NRs.

Interestingly, the activation energy for intermediate formation is significantly higher than that of Rf formation, further confirming the generation of AR· with higher energy barrier is the rate-limiting step of this fluorogenic reaction. Under illumination with 785 nm laser, activation energy of this step significantly decreased down to 42.4±1.6 kJ mol^{-1}, while the activation energies of final product generation and dissociation remained barely unchanged.

To further confirm the plasmon lowered E_a of intermediate, we interrogated

reductive N-deoxygenation of Resazurin to Resorufin under 785 nm laser illumination. In contrast to the plasmon enhancement, we observed negligible change in catalytic performance (Figure S7). These results clearly indicated that the plasmon enhanced catalytic performance originates from its ability of lowering the activation energy of rate-limiting step.

Table 1 Activation Energies of Tandem Reaction Steps at Dark or under Laser Illumination

	$<E_{a,\ off1}>$ (kJ mol^{-1})	$<E_{a,\ off2}>$ (kJ mol^{-1})	$<E_{a,on}>$ (kJ mol^{-1})
Under the dark	52.9 ± 3.8	5.5 ± 1.4	21.9 ± 3.2
Under illumination	42.4 ± 1.6	5.3 ± 1.3	21.4 ± 2.8

Compensation and Isokinetic Effect Interpreting the Role of Hot Carrier for the Enhanced Catalysis

Now, it is obvious that laser illumination accelerates the reaction rate by lowering the activation energy of intermediate product formation. A subsequent challenge is to reveal the contribution of hot carriers to the lowered activation energy.

Multiple possibilities have been proposed to explain the plasmon enhanced catalysis, including plasmon resulted heating of reaction surroundings (photothermal effect)[28-30], plasmon-induced changes of nanocatalysts itself (morphology and active site rearrangement)[31-32] and hot carriers facilitated reactant-catalyst interaction.[33-35] We carried out several control experiments to measure the surface temperature of Au NRs during laser irradiation (Figure S8) and its morphology after the plasmonic photocatalysis (Figure S9), and found negligible temperature and morphology change, thus possible contributions from photothermal effect and morphology were ruled out. In addition, the surface re-arrangement of catalyst is closely correlated with its fluctuations of activity, we thereby calculated the temporal fluctuations of activity of Au NRs under laser irradiation and found ignorable changes (Figure S10).[13] Therefore, we speculated the contribution of plasmon enhancement is not from the catalyst itself, but originated from the improved interactions between catalysts and substrates.

In transition state theory, activation energy of a chemical reaction is the saddle point of potential energy surface, and its value is depending on the vibrational energy stored in the bond.[36-38] The vibration frequency of a specific bond could be reflected by isokinetic temperature (T_{iso}) in isokinetic effect, which is related to, but not identical with compensation effect, a linear correlation between activation energy (E_a, which determines the temperature dependence) and frequency factor (A) in the Arrhenius dependence.[39-40] Compensation and isokinetic effect have been extensively observed in many thermal activated heterogeneous catalytic reactions, and are considered involve valuable information about the enthalpy and entropy changes of a reaction.[41-42] The validity of compensation and isokinetic effect at the single particle level has been demonstrated by Xu *et al*,[20] however, its validity in photocatalysis reaction is still uncertain.

Exner had suggested that when $T_1/T_2 \approx 1$, the compensation effect could be more reliably checked by plotting $\ln k_{i,1}$ *vs* $\ln k_{i,2}$.[43] In the present product formation process, the rate constant k_i represents the effective rate constants of intermediate product formation. $k_{i,1}$ and $k_{i,2}$ are the values of the rate constant k_i at two random temperatures T_1 and T_2, respectively ($T_1>T_2$). In both dark reaction and laser illumination, $\ln\gamma_{eff1,1}$ was positively correlated to $\ln\gamma_{eff1,2}$ (Figure 4A and B), indicating that the activation parameters indeed compensate one another and the compensation effect is also applicable to photocatalysis.

To further confirm the lower activation energy by plasmon exciting, the isokinetic (or isoequilibrium) temperature (T_{iso}), the special temperature that all the reactions in the series should have same rate (or equilibrium) constant, have also been investigated. We divided the individual gold nanorod into three subgroups according to the values of the activation energies. The dividing subgroups of individual gold nanorod were based on the following: for dark reaction small group: $44 \le E_{a,\,off1} < 49$ kJ mol^{-1}; middle group: $49 \le E_{a,\,off1} < 54$ kJ mol^{-1}; large group: $54 \le E_{a,\,off1} < 59$ kJ mol^{-1}. For laser illumination, small group: $39 \le E_{a,\,off1} < 42$ kJ mol^{-1}; middle group: $42 \le E_{a,\,off1} < 45$ kJ mol^{-1}; large group: $45 \le E_{a,\,off1} < 48$ kJ mol^{-1}. For each group, $\ln\gamma_{eff1}$ (where the rate

constant γ_{eff1} is an average over the entire subgroup) was plotted as a function of 1000/T. As shown in Figure 4C and D, for both dark reaction and under laser illumination, three independent plots intersect at one point. This indicates that an isokinetic relationship exists in photocatalysis. Compared to dark reaction (T_{iso}= 316 K), the T_{iso} for laser illumination (T_{iso}=314 K) reduced 2K, which probably indicates the substrate with lower energy barrier to convert into intermediate under laser illumination. We thus speculated that the plasmon excited electrons can induce multiple vibrational transitions of the Au-O bond that increases vibrational energy stored in the bond (Figure S11).[1] As a result, T_{iso} was reduced owing to the lowered activation energy.

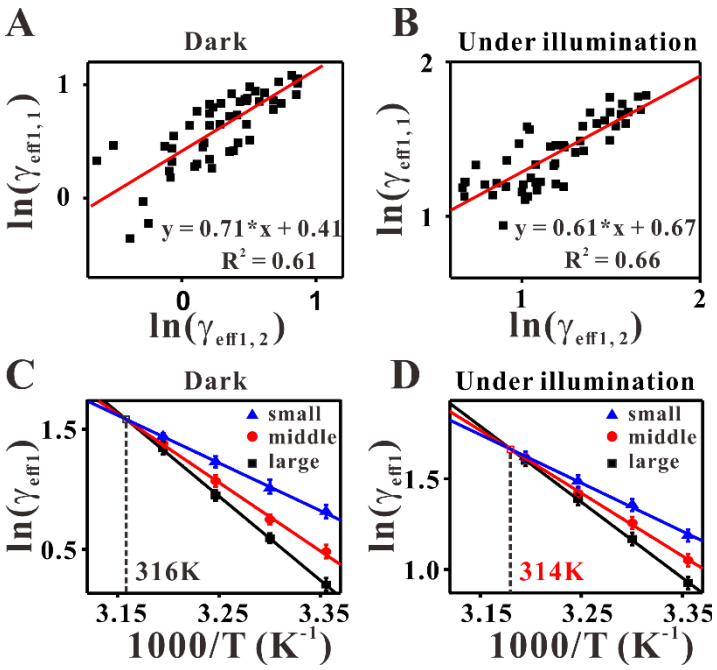

Figure 4 Compensation and isokinetic effect in the single-molecule photocatalysis of individual Au NR. Dependence of kinetic rate constants on individual Au NR at two temperatures for dark reaction and laser illumination (T_1, T_2, $T_1 > T_2$, here, T_1: {303 K, 308 K; 313 K}; T_2: {298 K, 303 K; 308 K}). Red lines are linear fits with R^2 = 0.61 (A) and R^2 = 0.66 (B). Isokinetic relationship of three groups of single gold nanorod with different average $E_{a,\,off1}$ in the coordinates 1000/T and lnγ_{eff1} for dark reaction (C) and laser illumination (D). Three groups for (C): small group: 44 ≤ $E_{a,\,off1}$ < 49 kJ mol^{-1} (blue); middle group: 49 ≤ $E_{a,\,off1}$ < 54 kJ mol^{-1} (red); large group: 54 ≤ $E_{a,\,off1}$ < 59 kJ mol^{-1} (black). Three groups for (D): small group: 39 ≤ $E_{a,\,off1}$ < 42 kJ mol^{-1} (blue); middle group: 42 ≤ $E_{a,\,off1}$ < 45 kJ mol^{-1} (red); large group: 45 ≤ $E_{a,\,off1}$ < 48 kJ mol^{-1} (black). The solid lines are the linear fittings.

Conclusions

In summary, we have proposed a single molecular strategy to derive rate-limiting step and activation energy of a plasmonic catalysis reaction by monitoring the temperature-dependent catalytic activity. The reason of plasmon enhancement was attributed to its ability to lower E_a of the rate-limiting step. Of note in the present fluorogenic reaction example, the rate-limiting step is the intermediate product generation, however, the strategy could be expanded to other plasmon enhanced reactions to derive rate-limiting steps. This ability provides new insight into exploring the mechanism of plasmonic catalysis, which deepens our understanding of plasmonic reaction and facilities designing desirable plasmon catalysts.

ASSOCIATED CONTENT

Supporting Information

The Supporting Information is available free of charge on the ACS Publications website at DOI:xxxxxxxxxx.

Experimental section and all control experiments availability.

AUTHOR INFORMATION

Corresponding Author：*E-mail: dli@chem.ecnu.edu.cn

ORCID

Di Li: 0000-0003-1674-0110

Notes

The authors declare no competing financial interest

ACKNOWLEDGMENTS

This work was supported by NSFC (21675166, 21874046, 21902050) and National Postdoctoral Program for Innovative Talents (BX20190118). The Shanghai Municipal Commission for Science and Technology (19JC1411800).

REFERENCES

(1) Zhou, L.; Swearer, D. F.; Zhang, C.; Robatjazi, H.; Zhao, H.; Henderson, L.; Dong, L.; Christopher, P.; Carter, E. A.; Nordlander, P.; Halas, N. J., Quantifying Hot Carrier and Thermal Contributions in Plasmonic Photocatalysis. *Science* **2018**, *362*, 69-72.

(2) Aslam, U.; Rao, V. G.; Chavez, S.; Linic, S., Catalytic Conversion of Solar to Chemical Energy on Plasmonic Metal Nanostructures. *Nat. Catal.* **2018**, *1*, 656-665.

(3) Aslam, U.; Chavez, S.; Linic, S., Controlling Energy Flow in Multimetallic Nanostructures for Plasmonic Catalysis. *Nat. Nanotechnol.* **2017**, *12*, 1000-1005.

(4) Liu, X.; Iocozzia, J.; Wang, Y.; Cui, X.; Chen, Y.; Zhao, S.; Li, Z.; Lin, Z., Noble Metal–Metal Oxide Nanohybrids with Tailored Nanostructures for Efficient Solar Energy Conversion, Photocatalysis and Environmental Remediation. *Energy Environ. Sci.* **2017**, *10*, 402-434.

(5) Peng, T.; Miao, J.; Gao, Z.; Zhang, L.; Gao, Y.; Fan, C.; Li, D., Reactivating Catalytic Surface: Insights into the Role of Hot Holes in Plasmonic Catalysis. *Small* **2018**, *14*, e1703510.

(6) Brongersma, M. L.; Halas, N. J.; Nordlander, P., Plasmon-Induced Hot Carrier Science and Technology. *Nat. Nanotechnol.* **2015**, *10*, 25-34.

(7) Zhan, C.; Chen, X.-J.; Yi, J.; Li, J.-F.; Wu, D.-Y.; Tian, Z.-Q., From Plasmon-Enhanced Molecular Spectroscopy to Plasmon-Mediated Chemical Reactions. *Nat. Rev. Chem.* **2018**, *2*, 216-230.

(8) Sivan, Y.; Baraban, J.; Un, I. W.; Dubi, Y., Comment on "Quantifying Hot Carrier and Thermal Contributions in Plasmonic Photocatalysis". *Science* **2019**, *364*, eaaw9367.

(9) Yen, C.-W.; El-Sayed, M. A., Plasmonic Field Effect on the Hexacyanoferrate (III)-Thiosulfate Electron Transfer Catalytic Reaction on Gold Nanoparticles: Electromagnetic or Thermal? *J. Phys. Chem.C* **2009**, *113*, 19585-19590.

(10) Kim, Y.; Smith, J. G.; Jain, P. K., Harvesting Multiple Electron-Hole Pairs Generated through Plasmonic Excitation of Au Nanoparticles. *Nat. Chem.* **2018**, *10*, 763-769.

(11) Xiao, Q.; Sarina, S.; Jaatinen, E.; Jia, J.; Arnold, D. P.; Liu, H.; Zhu, H., Efficient Photocatalytic Suzuki Cross-Coupling Reactions on Au–Pd Alloy Nanoparticles under Visible Light Irradiation. *Green Chem.* **2014**, *16*, 4272-4285.

(12) Xiao, Q.; Sarina, S.; Bo, A.; Jia, J.; Liu, H.; Arnold, D. P.; Huang, Y.; Wu, H.; Zhu, H., Visible Light-Driven Cross-Coupling Reactions at Lower Temperatures Using a Photocatalyst of Palladium and Gold Alloy Nanoparticles. *ACS Catal.* **2014**, *4*, 1725-1734.

(13) Xu, W.; Kong, J. S.; Yeh, Y. T.; Chen, P., Single-Molecule Nanocatalysis Reveals Heterogeneous Reaction Pathways and Catalytic Dynamics. *Nat. Mater.* **2008**, *7*, 992-996.

(14) Mao, X. W.; Liu, C. M.; Hesari, M.; Zou, N. M.; Chen, P., Super-Resolution Imaging of Non-Fluorescent Reactions via Competition. *Nat. Chem.* **2019**, *11*, 687-694.

(15) Zhou, X.; Andoy, N. M.; Liu, G.; Choudhary, E.; Han, K. S.; Shen, H.; Chen, P., Quantitative Super-Resolution Imaging Uncovers Reactivity Patterns on Single Nanocatalysts. *Nat. Nanotechnol.* **2012**, *7*, 237-241.

(16) Andoy, N. M.; Zhou, X.; Choudhary, E.; Shen, H.; Liu, G.; Chen, P., Single-Molecule Catalysis Mapping Quantifies Site-Specific Activity and Uncovers Radial Activity Gradient on Single 2D Nanocrystals. *J. Am. Chem. Soc.* **2013**, *135*, 1845-1852.

(17) Xu, Y.; Gao, Y. J.; Su, Y. Y.; Sun, L. L.; Xing, F. F.; Fan, C. H.; Li, D., Single-Molecule Studies of Allosteric Inhibition of Individual Enzyme on a DNA Origami Reactor. *J. Phys. Chem. Lett.* **2018**, *9*, 6786-6794.

(18) Liu, X.; Chen, T.; Xu, W., Revealing the Thermodynamics of Individual Catalytic Steps based on Temperature-Dependent Single-Particle Nanocatalysis. *Phys. Chem. Chem. Phys.* **2019,** *21*, 21806-21813.

(19) Chen, T.; Chen, S.; Song, P.; Zhang, Y.; Su, H.; Xu, W.; Zeng, J., Single-Molecule Nanocatalysis Reveals Facet-Dependent Catalytic Kinetics and Dynamics of Pallidium Nanoparticles. *ACS Catal.* **2017**, *7*, 2967-2972.

(20) Chen, T.; Zhang, Y.; Xu, W., Single-Molecule Nanocatalysis Reveals Catalytic Activation Energy of Single Nanocatalysts. *J. Am. Chem. Soc.* **2016**, *138*, 12414-12421.

(21) Christopher, P.; Moskovits, M., Hot Charge Carrier Transmission from Plasmonic Nanostructures. *Annu. Rev. Phys. Chem.* **2017**, *68*, 379-398.

(22) Kale, M. J.; Christopher, P., Plasmons at the Interface. *Science* **2015**, *349*, 587-588.

(23) Cordes, T.; Blum, S. A., Opportunities and Challenges in Single-Molecule and Single-Particle Fluorescence Microscopy for Mechanistic Studies of Chemical Reactions. *Nat. Chem.* **2013**, *5*, 993-999.

(24) Shen, H.; Zhou, X.; Zou, N.; Chen, P., Single-Molecule Kinetics Reveals a Hidden Surface Reaction Intermediate in Single-Nanoparticle Catalysis. *J. Phys. Chem.C* **2014**, *118*, 26902-26911.

(25) Janssen, K. P. F.; De Cremer, G.; Neely, R. K.; Kubarev, A. V.; Van Loon, J.; Martens, J. A.; De Vos, D. E.; Roeffaers, M. B. J.; Hofkens, J., Single Molecule Methods for the Study of Catalysis: from Enzymes to Heterogeneous Catalysts. *Chem. Soc. Rev.* **2014**, *43*, 990-1006.

(26) Xu, W. L.; Kong, J. S.; Chen, P., Single-Molecule Kinetic Theory of Heterogeneous and Enzyme Catalysis. *J. Phys. Chem.C* **2009**, *113*, 2393-2404.

(27) Xu, W. L.; Shen, H.; Kim, Y. J.; Zhou, X. C.; Liu, G. K.; Park, J.; Chen, P., Single-Molecule Electrocatalysis by Single-Walled Carbon Nanotubes. *Nano Lett.* **2009**, *9*, 3968-3973.

(28) Long, R.; Rao, Z. L.; Mao, K. K.; Li, Y.; Zhang, C.; Liu, Q. L.; Wang, C. M.; Li, Z. Y.; Wu, X. J.; Xiong, Y. J., Efficient Coupling of Solar Energy to Catalytic Hydrogenation by Using Well-Designed Palladium Nanostructures. *Angew. Chem., Int. Ed.* **2015**, *54*, 2425-2430.

(29) Yang, H.; He, L. Q.; Hu, Y. W.; Lu, X.; Li, G. R.; Liu, B.; Ren, B.; Tong, Y.; Fang, P. P., Quantitative Detection of Photothermal and Photoelectrocatalytic Effects Induced by SPR from Au@Pt Nanoparticles. *Angew. Chem., Int. Ed.* **2015**, *54*, 11462-11466.

(30) Karam, T. E.; Smith, H. T.; Haber, L. H., Enhanced Photothermal Effects and Excited-State Dynamics of Plasmonic Size-Controlled Gold–Silver–Gold Core–Shell–Shell Nanoparticles. *J. Phys. Chem.C* **2015**, *119*, 18573-18580.

(31) Gong, M. G.; Jin, X.; Sakidja, R.; Ren, S. Q., Synergistic Strain Engineering Effect of Hybrid Plasmonic, Catalytic, and Magnetic Core-Shell Nanocrystals. *Nano Lett.* **2015**, *15*, 8347-8353.

(32) Ye, Z. J.; Wei, L.; Xiao, L. H.; Wang, J. F., Laser Illumination-Induced Dramatic Catalytic Activity Change on Au Nanospheres. *Chem. Sci.* **2019**, *10*, 5793-5800.

(33) Guo, J.; Zhang, Y.; Shi, L.; Zhu, Y.; Mideksa, M. F.; Hou, K.; Zhao, W.; Wang, D.; Zhao, M.; Zhang, X.; Lv, J.; Zhang, J.; Wang, X.; Tang, Z., Boosting Hot Electrons in Hetero-Superstructures for Plasmon-Enhanced Catalysis. *J. Am. Chem. Soc.* **2017**, *139*, 17964-17972.

(34) Mukherjee, S.; Libisch, F.; Large, N.; Neumann, O.; Brown, L. V.; Cheng, J.; Lassiter, J. B.; Carter, E. A.; Nordlander, P.; Halas, N. J., Hot Electrons Do the Impossible: Plasmon-Induced Dissociation of H_2 on Au. *Nano Lett.* **2013**, *13*, 240-247.

(35) Boerigter, C.; Campana, R.; Morabito, M.; Linic, S., Evidence and Implications of Direct Charge Excitation as the Dominant Mechanism in Plasmon-Mediated Photocatalysis. *Nat. Commun.* **2016**, *7*,

10545.
(36) Dellago, C.; Bolhuis, P. G.; Csajka, F. S.; Chandler, D., Transition Path Sampling and the Calculation of Rate Constants. *J. Chem. Phys.* **1998**, *108*, 1964-1977.
(37) Shan, X.; Burd, T. A. H.; Clary, D. C., New Developments in Semiclassical Transition-State Theory. *J. Phys. Chem. A* **2019**, *123*, 4639-4657.
(38) Bao, J. L.; Truhlar, D. G., Variational Transition State Theory: Theoretical Framework and Recent Developments. *Chem. Soc. Rev.* **2017**, *46*, 7548-7596.
(39) Liu, L.; Guo, Q.-X., Isokinetic Relationship, Isoequilibrium Relationship, and Enthalpy-Entropy Compensation. *Chem. Rev.* **2001,** *101*, 673-696.
(40) Linert, W., The Isokinetic Relationship. *Chem. Soc. Rev.* **1989,** *18*, 477-505.
(41) Andreasen, A.; Vegge, T.; Pedersen, A. S., Compensation Effect in the Hydrogenation/Dehydrogenation Kinetics of Metal Hydrides. *J. Phys. Chem. B* **2005,** *109*, 3340-3344.
(42) Ruthven, D. M., The Compensation Effect in Chemical Kinetics. *Ind. Eng. Chem. Fundam.* **1973,** *12*, 262-262.
(43) Cremer, E., The Compensation Effect in Heterogeneous Catalysis. *Adv. Catal.* **1955**, *7*, 75-91.

TOC Figure

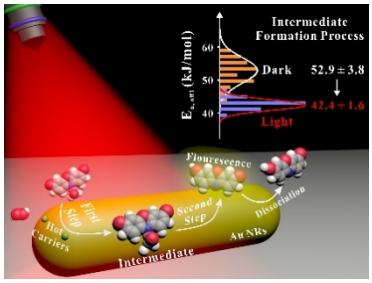
Intermediate
Formation Process
$E_{a,cat}$ (kJ/mol)
60
50
40
Dark
52.9 ± 3.8
42.4 ± 1.6
Light
Fluorescence
First
Step
Second
Step
Dissociation
Hot
Carriers
Intermediate
Au NRs